ChemComm

COMMUNICATION

Polymer micelle-directed growth of BaCO$_3$ spiral nanobelts†

Wenjie Zhu, Chunhua Cai, Jiaping Lin,* Liquan Wang, Lili Chen and Zeliang Zhuang

We discovered that micelles of a thermo-responsive polypeptide-based copolymer are able to direct growth of barium carbonate (BaCO$_3$) in the form of nanobelts. The BaCO$_3$ nanobelts tend to grow around a formed crystal, and curl into a spiral superstructure.

Shape- and size-controlled growth of inorganic materials has stimulated great research interest due to their potential applications in fields such as catalysis, medicine, electronics, ceramics, pigments and cosmetics.[1] Spiral and helical architectures are intriguing and ubiquitous in nature. Recently, the synthesis of helical inorganic materials such as barium sulfate, potassium dichromate, calcium, strontium and barium carbonates has been reported.[2,3] Reports on the spirals are very limited, indicating that the controlled synthesis of the spiral structures is still a challenge in inorganic chemistry.[4]

In biological systems, living organisms exert exceptional control over the gross morphology and nanoscale organization of biominerals, endowing them with fascinating properties.[5] One biomimetic mineralization synthesis strategy is to use transient amorphous precursors or liquid precursors.[6] An advantage of this strategy is that the precursors can adapt to complex shapes after being filled into templates. The polymer-induced liquid-precursor (PILP) phase is a highly hydrated, amorphous mineral precursor, first observed for calcium carbonate (CaCO$_3$) in systems containing anionic polymers.[7] The liquid precursor pathway is a promising method for preparing minerals with complex shapes.[8,9] For example, the PILP phase of CaCO$_3$ was used to infiltrate into porous polycarbonate membranes for capillary action, and subsequently crystallized into rod-like calcite single crystals.[9] However, there are only rare reports in the existing literature of generating complex structures from liquid precursors in the absence of exterior hard templates.[3]

Herein, we report for the first time that the barium carbonate (BaCO$_3$) can form spiral nanobelts in a biomimetic mineralization procedure under control of polymer micelles of poly(N-isopropyl propylacrylamide)-b-poly(L-glutamic acid) (PNIPAM-b-PLGA). The BaCO$_3$ has attracted much attention

Shanghai Key Laboratory of Advanced Polymeric Materials, State Key Laboratory of Bioreactor Engineering, Key Laboratory for Ultrafine Materials of Ministry of Education, School of Materials Science and Engineering, East China University of Science and Technology, Shanghai 200237, China. E-mail: jlin@ecust.edu.cn; Fax: +86 21-6425-1644
† Electronic supplementary information (ESI) available: The polymer synthesis, characterization, the micelle morphology, SEM images and XRD spectra of the carbonate crystals. See DOI: 10.1039/c2cc33197g

for its crystal structure is similar to an important biomineral aragonite, and it has many industrial applications, such as pigment, optical glass and electric condensers. The crystallization was carried out through a gas diffusion procedure, starting with a PNIPAM-b-PLGA–BaCl$_2$ mixed solution with 1.0 g L^{-1} polymer and 5 mM BaCl$_2$.[10] Raising the temperature of the mixed solution to 50 °C, which is above the low-critical solution temperature (LCST) of the PNIPAM segment, leads to the formation of spherical micelles (Fig. S1, ESI†). Crystallization was induced by slow diffusion of ammonium carbonate vapor into the solution. The precipitates were washed with water and allowed to dry for further examination. As shown in Fig. S2 (ESI†), the X-ray diffraction (XRD) pattern of the samples exhibits only orthorhombic witherite reflections with calculated lattice constants $a = 6.43$, $b = 5.32$ and $c = 8.90$ Å (JCPDS 45-1471).

The morphology of the samples was examined by scanning electron microscopy (SEM). Fig. 1a shows two kinds of structures, spirals and clumps, existing in the witherite products. A close inspection of Fig. 1a reveals that the spirals are constructed from crystal belts, and the spirals can have up to eight circles (Fig. 1b and c). The diameters of the spirals are typically 0.3–1.0 µm. The belt consists of spicules, roughly aligned parallel to one another. The clumps have irregular shapes with fibers as attached tentacles. In addition, some
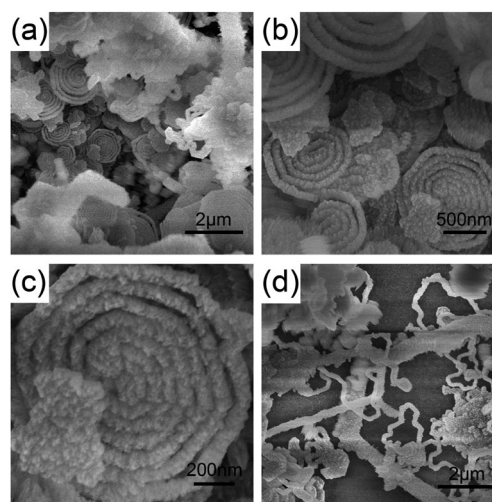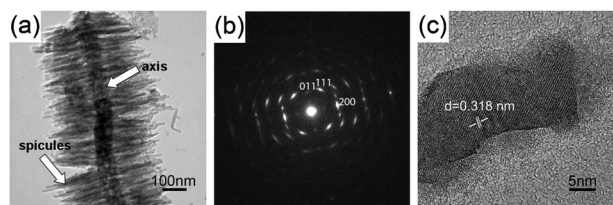

Fig. 1 SEM images of BaCO$_3$ crystals prepared in the PNIPAM-b-PLGA micelle solution at 50 °C after 24 hours of reaction. The concentration of BaCl$_2$ is 5 mM.

Fig. 2 (a) TEM image of part of a formed spiral belt. The arrow on the left side points to the spicules, while the arrow on the right side points to the axis. (b) The SAED pattern of the belt. (c) TEM image of a single spicule.

fibers with diameter of several hundred nanometers can also be discerned in the sample (Fig. 1d). The polymer content in the witherite samples is around 3.9%, according to the thermogravimetry analysis shown in Fig. S3 (ESI†). In a control experiment, only dendritic crystals were obtained in the absence of additives under similar conditions (results not shown). Dendritic crystals instead of spirals are generated in the polymer solution at 25 °C (Fig. S4, ESI†). These results indicate that the polymer micelles play a crucial role in the formation of $BaCO_3$ spirals.

The nanostructure and growth orientation of the crystals were further examined by using transmission electron microscopy (TEM) and selected-area electron diffraction (SAED) patterns. Fig. 2a shows a short, laid out piece of the belts. The formed fishbone-like structure featuring parallelly arranged spicules along the thick axis is in line with the results from SEM observations. The axis in the middle of the belt is a dark backbone and does not have regular crystal shape. The corresponding SAED pattern of the belt can be indexed as the $[01\bar{1}]$ zone axis (Fig. 2b). The arc SAED pattern reveals that the belt is a polycrystalline structure with the high crystallographic orientation. The TEM image of an individual spicule reveals that the lattice fringes are separated by about 0.318 nm distance, which corresponds to a lattice spacing of (200) in witherite (Fig. 2c). Both the TEM and SAED patterns indicate that the spicule grows preferentially along the *a*-axis. For the $BaCO_3$ belt, the symmetrical distribution of the spicules on both sides of the axis indicates that the spicules grow from the axis, and their orientation is regulated by isoepitaxy.[11]

Next, the polymer and Ba^{2+} concentrations were varied to investigate their influence on the $BaCO_3$ morphology (Fig. S5, ESI†). At a fixed polymer concentration of 1.0 g L^{-1}, the $BaCO_3$ morphology transforms from parallel rods to fibers as the Ba^{2+} concentration decreases from 20 to 2 mM. At a fixed Ba^{2+} concentration of 5 mM, the $BaCO_3$ morphology changes from the fibers to the spirals and then to the rods with decreasing micelle concentration. This continuous morphology evolution indicates that the spiral nanobelt integrates the features of both fiber and rod.

Fibers of alkali earth metal carbonate, including $CaCO_3$, $SrCO_3$ and $BaCO_3$, have recently been prepared through a so-called solution-precursor-solid (SPS) process associated with the PILP mechanism.[12,13] In the SPS process, a growth point is created from the PILP droplets, which contains a high concentration of ionic reactants. And the spatial constraint of the growth point leads to one-dimensional growth of the crystals. In a previous work, we have found that the
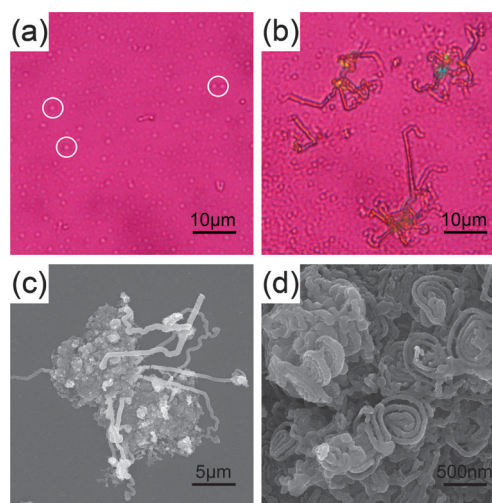

Fig. 3 POM (a and b, using first-order red gypsum λ-plate) and SEM (c and d) images of the $BaCO_3$ product after different reaction times, (a) 15 min and (b–d) 30 min.

PNIPAM-*b*-PLGA micelles can induce the generation of the PILP phase of $CaCO_3$.[14] The micelles mediated the formation of coral-like aragonite fibers at a high concentration through the SPS process.

To study the growth pattern in the $BaCO_3$ system, samples obtained at the initial reaction stage were observed by using a polarized optical microscope (POM) and SEM (Fig. 3). Fig. 3a displays the POM image of the sample after 15 minutes of reaction. The image shows many droplets with diameters of about one micrometer as marked by the white circles. The droplets are amorphous, judging from the lack of birefringence. After 30 minutes, fibers with tens of micrometers in length are observed and droplet-like growth tips can also be discerned (Fig. 3b). The SEM image shows that spiral belts coexisting with the fibers are formed at this stage (Fig. 3c and d). Thus, it is clear that the PILP phase exists at the initial crystallization stage and then crystallizes into fibers and spiral belts *via* the SPS process.

To clarify the mechanism underlying the micelle mediated mineralization, a few Mg^{2+} and Sr^{2+} ions were also added to the $BaCO_3$ system. The addition of Mg^{2+} and Sr^{2+} in a $CaCO_3$ crystallization system can enhance the PILP process by inhibiting solution crystal nucleation.[12] In contrast to the nanorods formed at a Ba^{2+} concentration of 10 mM, spiral belts are obtained by adding 1 mM Mg^{2+} or Sr^{2+} (Fig. S6, ESI†). This translation agrees well with our prediction that an enhanced PILP process improves one-dimensional growth. Observation of the spirals formed in the Ba–Sr system offers more insight into the growth process of the spirals. One characteristic of the spirals is that they tend to wind around the crystals which are formed in advance to duplicate the overall shapes (Fig. S7a, ESI†), or lead to the formation of a group of parallel belts (Fig. S7b, ESI†). Another characteristic is that the spirals can occasionally alter their directions (Fig. S7c, ESI†). Especially, the inversion always occurs when the belt hits an obstacle such as the surface of a glass slide (Fig. S7d, ESI†).

To explain the growth of the spiral, we propose a possible mechanism in which the fibrous growth of the belt *via* the SPS
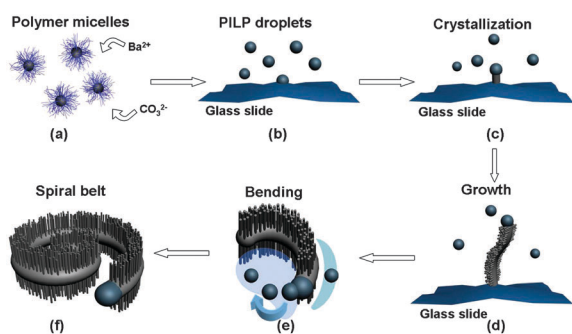
Scheme 1 Schematic image of the formation process of a spiral.

process can curve under diffusion-limited conditions (Scheme 1). In the solution, the micelle consists of a negatively charged PLGA corona and a hydrophobic PNIPAM core. In the initial stage, the coronas of the micelles sequester an excess of Ba^{2+} to form a complex due to the interaction between COO^- and Ba^{2+} (Scheme 1a).[15] With the continuous diffusion of CO_2, liquid precursors of $BaCO_3$ are constructed because the micelles can delay the crystallization of $BaCO_3$, as shown in the POM image in Fig. 3a and depicted in Scheme 1b. A further diffusion of CO_2 into the system leads to the deposition and crystallization of some precursor droplets (Scheme 1c). When the precursors coalesce with the underlying structure and crystallize, they serve as new growth points for anisotropic growth. Successive crystallization of the liquid precursors onto the growth tips leads to a fibrous growth of $BaCO_3$ (Fig. 3b).

From our knowledge of the PILP process, we know that the polymers dynamically migrate in the PILP process. The polymers first induce the PILP phase, then are excluded from the PILP phase to the solution during crystallization, and stimulate a secondary deposition of PILP phase.[16] Thus the excluded polymers can produce a concentration gradient of the liquid droplets around the formed crystals. Because the PILP phase is a viscous colloidal phase with a low mobility, an unevenly distributed PILP phase would be produced around formed crystals (shaded area, Scheme 1e).

In the spirals, the spicules arrayed in parallel can restrict the fibrous growth of the belt nearly in one plane. If the quantities of liquid precursors are unequal on both sides of a belt, the growth point will turn to the side with more precursors as the arrow shows in Scheme 1e. As a result, higher concentration polymers are excluded and stimulate more PILP phases on this side. The concentration gradient drive the growth direction always tilt to this direction.[17] Eventually, a spiral belt is formed (Scheme 1f). However, accidents may occur in the process, occasionally leading to an inversion of the rotation direction. The formation of the spiral should be in a proper condition coordinating the fibrous and bending growth. Otherwise, fibers and rods are formed more readily (see Scheme S1, ESI†).

In summary, we prepared $BaCO_3$ samples with an intriguing spiral belt morphology, the first example of such a structure in biomimetic mineralization systems. Based on the studies, we proposed a possible mechanism for elucidating the formation of a spiral belt, which adopts the SPS growth pattern under a diffusion-limited condition. The spiral pattern of $BaCO_3$ is similar to that of some minerals discovered in nature, for example, the spiral pattern of aragonite on the inner surface of nacre.[18] The present finding may help to explore the formation process of such a structure formed in biominerals. The spiral belts have no chirality and can occasionally alter their rotation direction. These phenomena may inspire other researchers to study the mechanism of chiral morphologies of many inorganic materials.

Notes and references

1 (a) S. Mann and G. A. Ozin, *Nature*, 1996, **382**, 313–318; (b) H. Yang, N. Coombs and G. A. Ozin, *Nature*, 1997, **386**, 692–695; (c) T. S. Ahmadi, Z. L. Wang, T. C. Green, A. Henglein and M. A. El-Sayed, *Science*, 1996, **272**, 1924–1925.

2 (a) M. Yang and N. A. Kotov, *J. Mater. Chem.*, 2011, **21**, 6775–6792; (b) Y. Oaki and H. Imai, *Cryst. Growth Des.*, 2003, **3**, 711–716; (c) T. Sugawara, Y. Suwa, K. Ohkawa and H. Yamamoto, *Macromol. Rapid Commun.*, 2003, **24**, 847–851; (d) T. Terada, S. Yamabi and H. Imai, *J. Cryst. Growth*, 2003, **253**, 435–444; (e) S. H. Yu, H. Cölfen, K. Tauer and M. Antonietti, *Nat. Mater.*, 2005, **4**, 51–55; (f) J. M. García-Ruiz, S. T. Hyde, A. M. Carnerup, A. G. Christy, M. J. Van Kranendonk and N. J. Welham, *Science*, 2003, **302**, 1194–1197.

3 (a) L. A. Gower and D. A. Tirrell, *J. Cryst. Growth*, 1998, **191**, 153–160; (b) J. H. Zhu, S. H. Yu, A. W. Xu and H. Cölfen, *Chem. Commun.*, 2009, 1106–1108.

4 (a) M. Li and S. Mann, *Langmuir*, 2000, **16**, 7088–7094; (b) J. M. García-Ruiz, *J. Cryst. Growth*, 1985, **73**, 251–262; (c) P. X. Gao and Z. L. Wang, *Small*, 2005, **1**, 945–949.

5 (a) J. Aizenberg, J. C. Weaver, M. S. Thanawala, V. C. Sundar, D. E. Morse and P. Fratzl, *Science*, 2005, **309**, 275–278; (b) F. C. Meldrum and H. Cölfen, *Chem. Rev.*, 2008, **108**, 4332–4432.

6 (a) J. Xiao and S. Yang, *Nanoscale*, 2012, **4**, 54–65; (b) D. Gebauer, P. N. Gunawidjaja, J. Y. P. Ko, Z. Bacsik, B. Aziz, L. Liu, Y. Hu, L. Bergström, C. W. Tai, T. K. Sham, M. Edén and N. Hedin, *Angew. Chem., Int. Ed.*, 2010, **49**, 8889–8891; (c) C. Cheng, Y. Yang, X. Chen and Z. Shao, *Chem. Commun.*, 2008, 5511–5513; (d) S. E. Wolf, J. Leiterer, V. Pipich, R. Barrea, F. Emmerling and W. Tremel, *J. Am. Chem. Soc.*, 2011, **133**, 12642–12649; (e) H. Pan, X. Y. Liu, R. Tang and H. Y. Xu, *Chem. Commun.*, 2010, **46**, 7415–7417.

7 (a) L. B. Gower and D. J. Odom, *J. Cryst. Growth*, 2000, **210**, 719–734; (b) L. B. Gower, *Chem. Rev.*, 2008, **108**, 4551–4627.

8 X. G. Cheng and L. B. Gower, *Biotechnol. Prog.*, 2006, **22**, 141–149.

9 Y. Y. Kim, N. B. J. Hetherington, E. H. Noel, R. Kröger, J. M. Charnock, H. K. Christenson and F. C. Meldrum, *Angew. Chem., Int. Ed.*, 2011, **50**, 12572–12577.

10 S. Albeck, S. Weiner and L. Addadi, *Chem.–Eur. J.*, 1996, **2**, 278–284.

11 H. Shi, L. Qi, J. Ma and H. Cheng, *J. Am. Chem. Soc.*, 2003, **125**, 3450–3451.

12 M. J. Olszta, S. Gajjeraman, M. Kaufman and L. B. Gower, *Chem. Mater.*, 2004, **16**, 2355–2362.

13 S. J. Homeijer, R. A. Barrett and L. B. Gower, *Cryst. Growth Des.*, 2010, **10**, 1040–1052.

14 W. Zhu, J. Lin and C. Cai, *J. Mater. Chem.*, 2012, **22**, 3939–3947.

15 W. Li, S. Sun, Q. Yu and P. Wu, *Cryst. Growth Des.*, 2010, **10**, 2685–2692.

16 L. Dai, E. P. Douglas and L. B. Gower, *J. Non-Cryst. Solids*, 2008, **354**, 1845–1854.

17 Y. Oaki and H. Imai, *Langmuir*, 2005, **21**, 863–869.

18 K. Wada, *Nature*, 1966, **211**, 1427.